High Intrarenal Lactate Production Inhibits the Renal Pseudohypoxic Response to Acutely Induced Hypoxia in Diabetes

Christoffer Laustsen[1], Kasper Lipsø[2,3], Jakob Appel Østergaard[4], Per Mose Nielsen[1], Lotte Bonde Bertelsen[1], Allan Flyvbjerg[5,6], Michael Pedersen[1], Fredrik Palm[7], and Jan Henrik Ardenkjær-Larsen[2,3,8]

[1]Department of Clinical Medicine, MR Research Centre, Aarhus University, Aarhus, Denmark; [2]Danish Research Centre for Magnetic Resonance, Copenhagen University Hospital Hvidovre, Hvidovre, Denmark; [3]Department of Electrical Engineering, Technical University of Denmark, Kgs Lyngby, Denmark; [4]Department of Endocrinology and Internal Medicine, Aarhus University Hospital, Aarhus, Denmark; [5]Steno Diabetes Center Copenhagen, The Capital Region of Denmark, Gentofte, Denmark; [6]University of Copenhagen, Copenhagen, Denmark; [7]Department of Medical Cell Biology, Uppsala University, Uppsala, Sweden; and [8]GE Healthcare, Copenhagen, Denmark

Corresponding Author:
Christoffer Laustsen, PhD
Aarhus University Hospital, MR Center, Palle Juul Jensens Boulevard.,
DK-8200 Aarhus N, Denmark;
E-mail: cl@clin.au.dk

Key Words: MRI, type 1-diabetes, kidney, renal metabolism, hyperpolarization
Abbreviations: Lactate dehydrogenase (LDH), pyruvate dehydrogenase (PDH), magnetic resonance imaging (MRI), blood oxygenation level–dependent (BOLD), magnetic resonance (MR), magnetic resonance spectroscopy (MRS), field of view (FOV), repetition time (TR), echo time (TE), chemical shift imaging (CSI)

ABSTRACT

Intrarenal hypoxia develops within a few days after the onset of insulinopenic diabetes in an experimental animal model (ie, a model of type-1 diabetes). Although diabetes-induced hypoxia results in increased renal lactate formation, mitochondrial function is well maintained, a condition commonly referred to as pseudohypoxia. However, the metabolic effects of significantly elevated lactate levels remain unclear. We therefore investigated in diabetic animals the response to acute intrarenal hypoxia in the presence of high renal lactate formation to delineate mechanistic pathways and compare these findings to healthy control animals. Hyperpolarized ^{13}C-MRI and blood oxygenation level–dependent ^{1}H-MRI was used to investigate the renal metabolism of [1-^{13}C]pyruvate and oxygenation following acutely altered oxygen content in the breathing gas in a streptozotocin rat model of type-1 diabetes with and without insulin treatment and compared with healthy control rats. The lactate signal in the diabetic kidney was reduced by 12%–16% during hypoxia in diabetic rats irrespective of insulin supplementation. In contrast, healthy controls displayed the well-known Pasteur effect manifested as a 10% increased lactate signal following reduction of oxygen in the inspired air. Reduced expression of the monocarboxyl transporter-4 may account for altered response to hypoxia in diabetes with a high intrarenal pyruvate-to-lactate conversion. Reduced intrarenal lactate formation in response to hypoxia in diabetes shows the existence of a different metabolic phenotype, which is independent of insulin, as insulin supplementation was unable to affect the pyruvate-to-lactate conversion in the diabetic kidney.

INTRODUCTION

In the diabetic kidney, hyperglycemia activates primarily mitochondrial uncoupling and secondarily the production of reactive oxygen species, which reduces energy production and creates hypoxia and an increased oxygen sensitivity in the kidney (1-5). Lactate dehydrogenase (LDH) and pyruvate dehydrogenase (PDH) are key enzymes in the pyruvate metabolism, thus facilitating pyruvate conversion to lactate or acetyl coenzyme A. Acetyl coenzyme A is the entry into Krebs cycle and follows the mitochondrial respiratory chain. An unchanged PDH activity indicates sufficient oxygen supply to the diabetic kidney, while hypoxia causes an elevated lactate pool and possibly a reduced PDH activity (1, 6, 7).

Magnetic resonance imaging (MRI) is considered an important functional imaging method for clinical decision-making in patients with renal disease (8-11), as well as in preclinical animal studies (12-15). Particularly important to assess the metabolic balance (PDH versus LDH) are the blood oxygenation level–dependent (BOLD) method and the metabolic imaging approach referred to as hyperpolarized ^{13}C-based magnetic resonance (MR) spectroscopy (5, 16-19). The combination of these 2 methods enables longitudinal assessment of oxygen availability in parallel with PDH ([1-^{13}C]pyruvate-to-^{13}C-bicarbonate conversion) and LDH ([1-^{13}C]pyruvate-to-[1-^{13}C]lactate conversion) flux estimation directly in the kidney tissue in vivo (5). Previous studies have shown high and unaltered pyruvate-to-lactate conversion in the early diabetic kidney (3, 5, 20-24). This pyruvate-to-lactate conversion has previously been correlated with the severity of diabetic renal complications toward diabetic nephropathy (25). Interestingly, diabetic rats with similar pyru-

ISSN 2379-1381 https://doi.org/10.18383/j.tom.2019.00003

Table 1. RT-PCR Primer Sequences

Gene	Forward Sequence	Reverse Sequence
Rat 18S	5′-CAT GGC CGT TCT TAG TTG-3′	5′-CAT GCC AGA GTC TCG TTC-3′
Rat PDH-A1	5′-TCC ACT CCT TGT AGC TGC AAC-3′	5′-GAG AAC CCA CCA CCC CAT G-3′
Rat LDH-A	5′-GCC ATG TAT TCC TTC CCT CA-3′	5′-GCC TCA TTG AAG ACC TGC TC-3′
Rat ALT	5′-GCC ATG TAT TCC TTC CCT CA-3′	5′-GCC TCA TTG AAG ACC TGC TC-3′
Rat MCT-1	5′-CTC TGG GCG CCG CGA GAT AC-3′	5′-CAA CTA CCA CCG CCC AGC CC-3′
Rat MCT-4	5′-CCA GGC CCA CGG CAG GTT TC-3′	5′-GCC ACC GTA GTC ACT GGC CG-3

vate-to-lactate conversion to healthy controls under normoxic conditions showed an increased pyruvate-to-lactate conversion following acute reduction in the respired oxygen content (3). Moreover, treatment with insulin increased the overall metabolic conversion (not sufficient to maintain good glycemic control), including increased pyruvate-to-lactate conversion (20). These discrepancies seem to suggest either a large variation in the streptozotocin model or potential distinct metabolic phenotypes. In this study, we investigated the metabolism of diabetic rats exhibiting increased pyruvate-to-lactate conversion compared with previous reports at similar time points and similar conditions (2 weeks of diabetes), although similar or even less pronounced diabetic complications and as such represent a naturally occurring phenotype or variation with unknown origin. We study the response to acutely altered oxygen supply [66% O_2, sufficient oxygen to ensure fully saturated blood versus 10% O_2, low oxygen content similar to previous report (3)], with and without insulin supplementation. We test the hypothesis that severe pseudohypoxia [highly elevated lactate-to-pyruvate ratio compared with controls and aforementioned previous reports at 2 weeks (3, 20)] is unable to compensate the lack of oxygen by increasing the intracellular lactate and thus is exhibiting an alternative metabolic phenotype.

METHODOLOGY

Animals and Study Protocol

Twenty-two 8-week-old female Wistar rats (N = 7–8/group; Taconic, Ry, Denmark) were included in this study. The rats were kept in cages with a 12:12-h light–dark cycle, temperature of 21°C ± 2°C and a humidity of 55% ± 5%. Diabetes was induced by an intravenous injection of freshly prepared streptozotocin (55 mg/kg body weight; Sigma-Aldrich, St. Louis, MO) dissolved in 10 mmol/L cold citrate buffer (pH 4.5). Blood glucose was measured in tail capillary blood with a Contour blood glucose meter (Bayer Diabetes Care, Copenhagen, Denmark). Rats were considered diabetic when the blood glucose levels exceeded 15 mmol/L at 48 h after injection of streptozotocin. The rats were divided into a diabetes group and treated group after 1.5 weeks of diabetes. NPH insulin (Eli Lilly, IN) was administered subcutaneous daily for 3 days (1 IU morning and 3 IU afternoon) before the MRI examination. On the day of the MRI examination, the rats received 1 IU in the morning 2–4 h before the MRI scan. The study complied with the guidelines for use and care of laboratory animals and was approved by the Danish Inspectorate of Animal Experiments (License: 2010/561-1938).

Colorimetric Assays

Assays to measure LDH and PDH activity and the absolute amount of lactate were performed according to manufacturer's instructions (Sigma-Aldrich, St. Louis, MO). The assays were performed on homogenized tissue samples dissolved in buffer from each of the respective assays, derived from cortical kidney biopsies. Biopsies were obtained at the time of sacrifice and stored in −80°C. Absorbance was measured in 384 Costar well plates using a PHERAstar FS microplate reader (BMG Labtech, Birkerød, Denmark). In a full spectrum test screen, we found that the optimal wavelength was 662 nm for LDH, PDH, and lactate. The calculated activities were normalized to protein content in the kidney sample. Protein content was determined using a Qubit 3.0 fluorometer (Life Technologies, Thermo Fisher Scientific, Hvidovre, Denmark).

RNA Extraction and Quantitative Polymerase Chain Reaction

RNA extraction and qPCR were performed. In brief, total RNA was isolated using a Nucleospin RNA II kit (Strategene, AH Diagnostics, Aarhus, Denmark) following manufacturer's instructions. We measured RNA purity and concentration using a Qubit 3.0 fluorometer (Life Technologies). cDNA synthesis was performed on 0.5-μg RNA with the RevertAid first-strand cDNA synthesis kit following manufacturer's instructions (Thermo Fisher Scientific). Samples for qPCR were prepared using Maxima SYBR Green Master Mix following manufacturer's instructions (Thermo Fisher Scientific). The qPCR protocol comprised 40 cycles of denaturation for 30 seconds at 95°C followed by annealing and synthesis for 1 minute at 60°C. Rat primer sequences used are described in Table 1. As mentioned, kidneys were rapidly dissected after sacrifice. Cortex and inner medulla were isolated to tubes and dumped in liquid nitrogen and stored in −80°C. Cortex biopsies were homogenized for RNA extraction.

[1-^{13}C]Pyruvate Hyperpolarization

A volume of 20-μL [1-^{13}C]pyruvic acid (Sigma Aldrich) containing 15mM OX063 (Oxford Instruments, Oxford, UK) and 1.5 mmol/L Dotarem (Guerbet, Villepinte, France) was inserted into a dissolution-DNP HyperSense polarizer (Oxford Instruments Molecular Biotools, Oxford, UK). The sample was polarized for

1 h at 94.118 GHz (100 mW). The hyperpolarized sample was dissolved in 4 mL of a dissolution medium (80 mmol/L TRIS, 100 mg/L EDTA, 50 mmol/L NaCl, 80 mmol/L NaOH), yielding an isotonic 80 mmol/L [1-^{13}C]-pyruvate solution at physiological pH. The sample temperature after dissolution was 30°C–35°C, resulting in a reproducible polarization of 30% and a T1 in the range of 40–60 seconds (26). A volume of 1.0 mL was injected into the tail vein over 10 seconds. The transfer time between dissolution and injection was 10 seconds on average, and the ^{13}C chemical shift imaging (CSI) MR-sequence was initiated 20 seconds after start of injection.

Magnetic Resonance Imaging and Spectroscopy

Two weeks after induction of diabetes, tail vein catheterization was performed for administration of hyperpolarized [1-^{13}C]pyruvate. The animal was placed in a 4.7 T Agilent MR scanner with VnmrJ 4.0 (Agilent, Santa Clara, CA) that was equipped with a dual-tuned ^{1}H/^{13}C volume transmit and a 4-channel array surface receive-coil (Rapid Biomedical, Würzburg, Germany). The protocol (Figure 1) consists of 2 baseline scans (^{1}H BOLD MRI and a ^{13}C magnetic resonance spectroscopy [MRS]) during hyperoxic breathing with 66% oxygen content (0.8% isoflurane, 0.66 L/min oxygen, and 0.34 L/min nitrogen) and 2 postinterventions scans (^{1}H BOLD MRI and a ^{13}C MRS) with a 10% oxygen content (15 minutes of 0.8% isoflurane, 0.10 L/min oxygen, and 0.90 L/min nitrogen). Temperature and respiration were monitored. After the MRI session, a 5- to 7-mL blood sample was collected from the aortic bifurcation to EDTA-coated tubes for determination of plasma electrolytes.

MRI and MRS sequence parameters were as follows. An oxygenation-dependent (T2*-weighted) sequence was performed using an axial ^{1}H multiecho gradient-echo sequence. The sequence parameters were: matrix = 128 × 128, field of view (FOV) = 60 × 60 mm^2, flip angle = 30°, repetition time (TR) = 300 milliseconds, number of transients = 16, echo time (TE) = 2, 4, 6, 8, 10, 12, 14, 16 milliseconds, slices = 3, slice thickness = 5 mm, covering both kidneys. A scout ^{1}H axial gradient echo sequence (matrix = 128 × 128, FOV = 60 × 60 mm^2, TR/TE = 100 ms/2.6 ms, flip angle = 20°, averages = 16, slices = 7, slice thickness = 3 mm, covering both kidneys) was acquired for anatomical overlay. A slice-selective 2D ^{13}C chemical-shift imaging sequence was used for hyperpolarized [1-^{13}C]-pyruvate imaging. Parameters were chosen to be similar to previous studies in the same animal model (4, 20): flip angle = 10°, a centric circular k-space trajectory (169 phase encodings), TR/TE = 75 ms/0.65 ms, FOV = 60 × 60 mm^2, spectral width = 4000 Hz, data sampling = 256 complex points, and an axial slice thickness = 20 mm, covering both kidneys.

MRI Analysis

Data analysis of BOLD MRI data was performed in VnmrJ 4.0, generating R_2* maps. CSI data were processed in Matlab (MathWorks, Natick, MA). Spatial dimensions were apodized with a hamming function and zero-filled to a 32 × 32 grid. The spectral dimension was centered on the pyruvate frequency; apodized with a zero shifted sine-bell function and a 5-Hz exponential line broadening; and processed as sum-of-squares of the four coil channels. Spectral analysis was performed on a single voxel placed inside the kidney. Metabolite signals were integrated over a 60-Hz symmetric region. The metabolite signals were normalized relative to the total carbon signal.

Statistical Analyses

Normality was assessed with quantile plots. $P < .05$ was considered statistically significant. A 2-way repeated measurement analysis of variance (ANOVA) was used to compare the metabolic response as a function of oxygen availability between the three groups, using Sidak corrections for multiple comparisons. Statistical analysis was performed in PRISM. Statistical analysis of animal, kidney weight and blood glucose were analyzed with a 1-way ANOVA, while HbA_{1c} between the diabetics and the diabetics receiving insulin was analyzed using a 2-tailed Student t test with equal variance. The intrarenal lactate concentration variance was analyzed using a Brown–Forsyth test of variance.

RESULTS

All diabetic rats developed sustained hyperglycemia within 48 h. Body weight, kidney weight, and long-term glucose level HbA1c were comparable between diabetes and insulin-treated groups (Table 2). Renal oxygen availability depended on the inspired oxygen content, and BOLD MRI showed a significantly decreased T2* in the renal cortex in all groups following a reduction in the oxygen content of the breathing gas (diabetes group, diabetes + insulin group, and control group) ($P < .001$) (Figure 2). The medullary T2* was inversely correlated with oxygen content in the breathing gas in both the diabetes group ($P = .0009$) and in the diabetes + insulin group, albeit the latter did not reach significance ($P = .087$) (Figure 2). On the other hand, T2* was unaffected by altered oxygen availability in the control group ($P = .96$) (Figure 2). Both untreated diabetic ($P < .001$) and insulin-treated diabetic ($P < .001$) rats had an overall increased lactate production (lactate-to-total carbon ratio) in the kidneys compared with healthy controls. In both the untreated diabetes group ($P = .001$) and the insulin-treated diabetes group ($P = .004$), we found a decreased lactate-to-total carbon ratio in response to decreased oxygen availability, while the healthy controls ($P = .035$) showed a significantly increased lactate-to-total carbon ratio in response to decreased oxygen availability (Figure 3). The alanine and the bicarbonate-to-total carbon ratios were unaffected by altered oxygen supply in all groups (Figure 3). The pyruvate-to-total carbon ratio increased after administration of a low oxygen content in the diabetes group compared with controls ($P < .001$), and similar findings were found in the diabetes + insulin group ($P < .001$), while a tendency toward a decreased pyruvate signal was observed in the diabetes + insulin group ($P = .070$) (Figure 3). A statistically significant variance (Brown–Forsyth test, $P = .040$) was found in renal lactate concentration among the groups, indicating a significantly elevated lactate concentration in the 2 diabetes groups compared with controls (Figure 4).

A statistically significant difference in lactate dehydrogenase activity was found between both diabetes groups and the control group ($P = .001$), with the highest activity seen in the diabetes + insulin group, while no difference in LDH expression was seen between any of the groups (Figure 4). No difference

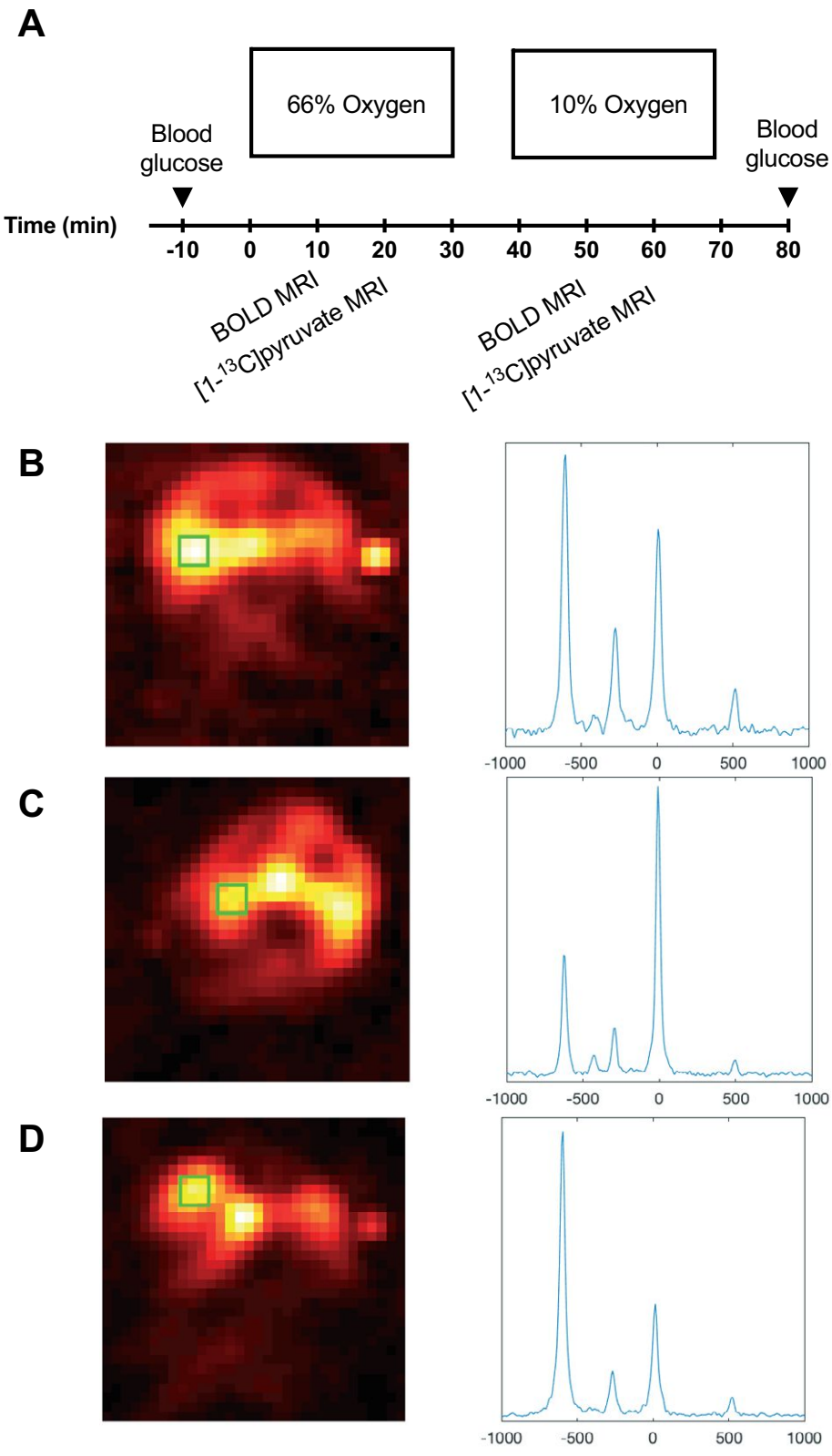

Figure 1. Study protocol (A). All animals were exposed to either 66% oxygen content or 10% oxygen content in the breathing gas. Blood oxygen level–dependent (BOLD) scan is performed 10 minutes after the change of oxygen content followed by a hyperpolarized ^{13}C pyruvate scan 20 minutes thereafter. Hyperpolarized ^{13}C chemical shift imaging (CSI) image of a healthy control animal and accompanying kidney spectra from the green region of interest (ROI) (B). Hyperpolarized ^{13}C CSI image of a untreated diabetic animal and accompanying kidney spectra from the green ROI (C). Hyperpolarized ^{13}C CSI image of an insulin-treated diabetic animal and accompanying kidney spectra from the green ROI (D).

Table 2. Animal Characteristics

	Body Weight (g)	Kidney Weight (g)	Blood Glucose (mmol/L)	HbA_{1c} (%)
Control	222 ± 7	0.8 ± 0.1	8.6 ± 0.7	Not measured
Diabetes	213 ± 20	1.1 ± 0.1[a]	23.8 ± 3.8[a]	11.4 ± 1.5
Diabetes + Insulin	200 ± 26	1.1 ± 0.2[a]	21.0 ± 4.0[a]	12.3 ± 0.7

[a]$P < 0.05$ versus control. The blood glucose level is the average blood glucose of the 2 measurements performed in each rat. Values are represented as mean ± SD. Comparisons analyzed using 1-way ANOVA and Student *t* test.

was seen in the lactate-to-bicarbonate, lactate-to-alanine, and alanine-to-bicarbonate ratios in untreated and insulin-treated diabetic rats during inspiration of 66% and 10% oxygen in the breathing gas (Figure 5). The pyruvate dehydrogenase activity increased in the untreated diabetes group, while the PDH expression was significantly decreased in both diabetes groups (Figure 6). Monocarboxylate transporters (MCT1) was found to be similar in all groups ($P = .27$), whereas MCT4 was found to be significantly reduced in both diabetes groups ($P < .001$) (Figure 6).

DISCUSSION

We have previously reported that the diabetic kidney responded with a pronounced increase in lactate formation following reduced oxygen availability compared with healthy controls (3). The decreased lactate formation in response to low oxygen availability observed in the present study is likely explained by the severity of diabetic nephropathy and the more increased lactate level (80% increased pyruvate-to-lactate conversion compared with previous reports (3, 20). The underlying mechanism for this altered metabolic phenotype is believed to originate from the altered expression of MCT4 in the diabetic rat kidney (dramatically downregulated) in response to profound lactate accumulation similar to what is observed in response to prolonged hypoxia (27). MCT1 controls the influx of lactate, whereas MCT4 ensures redox balance by export of lactate. Restricting lactic acid efflux from renal cells (maintained or reduced MCT4 expression) in concern with increased intracellular lactic acid accumulation, leading to an increased hyperpolarized [1-^{13}C]pyruvate-to-[1-^{13}C]lactate conversion (increased MCT1 expression in diabetes), might be a preventive mechanism to avoid systemic lactic acidosis, as seen in muscles, where an intracellular accumulation of lactic acid and subsequent altered redox state will inhibit glycolysis and induce muscle fatigue before systemic alterations to the pH regulation of the body (27, 28). Indeed mild acidosis has recently been associated with an altered metabolic phenotype in postmitotic cells, overriding oxygen deprivation and thus maintaining mitochondrial function (29). Taken together, an altered MCT transport is essential to the metabolic phenotype seen in diabetes, and an altered efflux of lactate could be the origin of this counterintuitive oxygen reversed oxygen sensitivity.

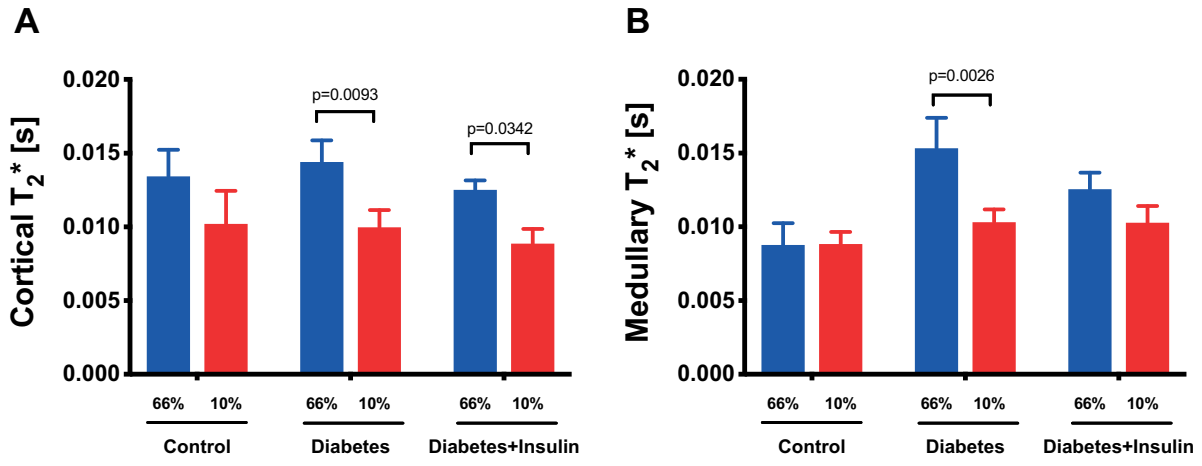

Figure 2. BOLD magnetic resonance imaging (MRI) in cortex and medulla of controls and untreated and insulin-treated diabetic rats during inspiration of 66% and 10% oxygen in the breathing gas. (**Cortical T2***) $P = .68$ for group (*between healthy controls* and *untreated and* insulin-treated *diabetic rats*), $P = .0001$* for treatment (*inspired oxygen*), and $P = .81$ for interaction (A). (**Medullary T2***) $P = .08$ for group (*between healthy controls* and *untreated and* insulin-treated *diabetic rats*), $P = .005$* for treatment (*Inspired oxygen*), and $P = .04$ for interaction* (B). Lines denote mean ± SEM. Two-way repeated ANOVA.

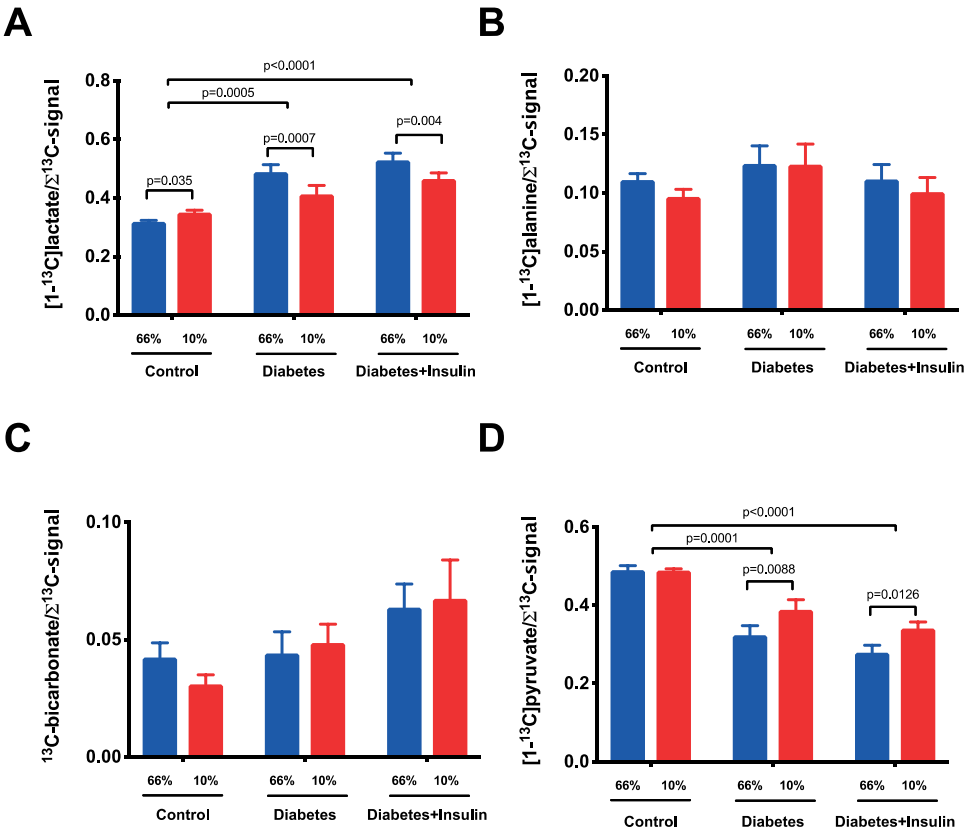

Figure 3. Hyperpolarized lactate, pyruvate, alanine, and bicarbonate signal to sum of the signal ratios in controls and untreated and insulin-treated diabetic rats during inspiration of 66% and 10% oxygen in the inspired air. (**Lactate-to-Σsignal**) $P < .001$ for group* (*between healthy controls* and *untreated and* insulin-treated *diabetic rats*), $P = .002$* for treatment (*inspired oxygen*), and $P = .0007$ for interaction* (A). (**Alanine-to-Σsignal**) $P = .43$ for group (*between healthy controls* and *untreated and* insulin-treated *diabetic rats*), $P = .15$ for treatment (*inspired oxygen*), and $P = .6$ for interaction (B). (**Pyruvate-to-Σsignal**) $P < .001$ for group* (*between healthy controls* and *untreated and* insulin-treated *diabetic rats*), $P = .002$ for treatment* (*inspired oxygen*), and $P = .05$ for interaction* (C); (**Bicarbonate-to-Σsignal**) $P = .1$ for group* (*between healthy controls* and *untreated and* insulin-treated *diabetic rats*), $P = .85$ for treatment* (*inspired oxygen*), and $P = .46$ for interaction. Two-way repeated ANOVA (D).

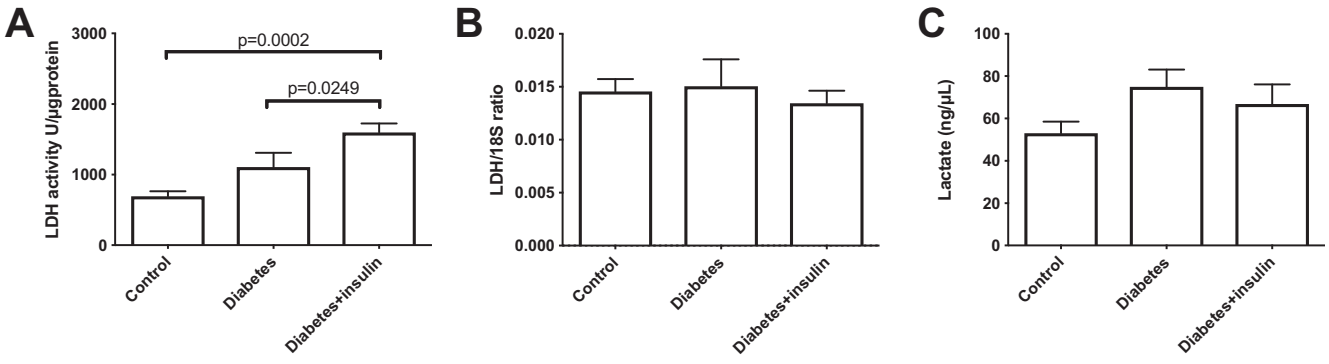

Figure 4. Colorimetric assay lactate dehydrogenase activity ($P = .001$) (A), qPCR lactate dehydrogenase mRNA expression ($P = .787$) (B), and colorimetric assay kidney tissue lactate concentration ($P = .187$) (C); significant variance (Brown–Forsyth test, $P = .04$) was found between healthy controls and untreated and insulin-treated diabetic rats. One-way ANOVA.

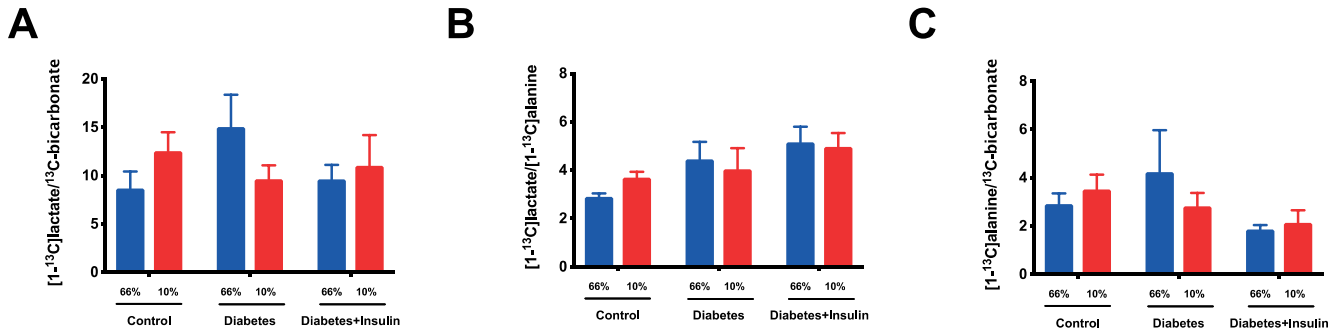

Figure 5. Hyperpolarized lactate-to-bicarbonate, lactate-to-alanine, and alanine-to-bicarbonate signal ratios in untreated and insulin-treated diabetic rats during inspiration of 66% and 10% oxygen in the inspired air. (**Lactate-to-Bicarbonate**) $P = .73$ for group (*between healthy controls* and *untreated and insulin-treated diabetic rats*), $P = .98$ for treatment (*inspired oxygen*), and $P = .06$ for interaction (A). (**Lactate-to-Alanine**) $P = .14$ for group (*between healthy controls* and *untreated and insulin-treated diabetic rats*), $P = .78$ for treatment (*inspired oxygen*), and $P = .12$ for interaction (B). (**Alanine-to-bicarbonate**) $P = .32$ for group (*between healthy controls* and *untreated and insulin-treated diabetic rats*), $P = .72$ for treatment (*Inspired oxygen*), and $P = .23$ for interaction (C). Two-way repeated ANOVA.

We speculate that the altered lactate transport could be active inhibition of the monocarboxylic transporters, as previously shown for the active mitochondrial pyruvate transporter with α-cyano-4-hydroxycinnamate (30) and in muscle tissue where lactate uptake and efflux stimulate an increased lactate concentration and altered intra- and extracellular pH (31).

Interestingly, the increased lactate-to-total carbon ratio in the diabetic kidney occurred regardless of insulin supplementation, indicating that insulin did not affect the balance between oxygen availability and energy metabolism in the hypoxic diabetic kidney. These findings support previous reports on increased lactate production in the diabetic kidneys regardless of

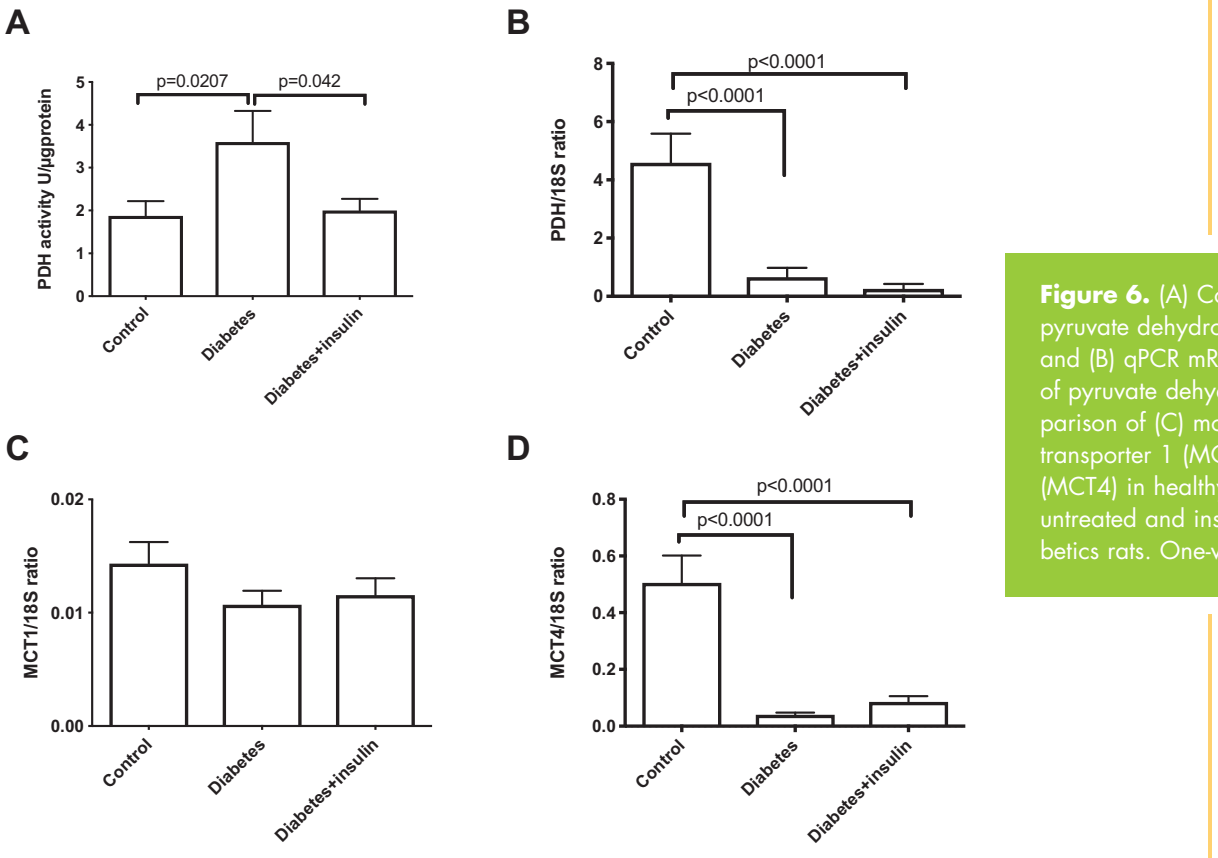

Figure 6. (A) Colorimetric assay pyruvate dehydrogenase activity and (B) qPCR mRNA expressions of pyruvate dehydrogenase; comparison of (C) monocarboxylate transporter 1 (MCT1) and (D) 4 (MCT4) in healthy controls and untreated and insulin-treated diabetics rats. One-way ANOVA.

insulin treatment (20). However, these results also imply the presence of different metabolic phenotypes occurring in diabetes, as high intrarenal lactate levels significantly altered the response to reduced oxygen availability in the diabetic animals (3, 4, 20, 25). This finding might be explained by the need for the high lactate-producing kidney to maintain homeostasis during hypoxia as previously reported in cancer cells (32). Thus, acute hypoxia in an already high lactate environment increases the lactate-to-pyruvate conversion and/or reduces the pyruvate-to-lactate conversion and thus maintains the intracellular redox potential. It is unlikely that the difference in the metabolic conversion is due to decreased conversion in diabetic rats, as the pyruvate-to-total carbon ratio was lower (ie, more pyruvate is being converted to its metabolic derivatives) in diabetics compared with controls.

The increased pyruvate-to-lactate conversion may characterize the severity of the deranged metabolism in the diabetic kidney, as previously described by Lin et al. (33). However, the increased lactate-to-pyruvate level found in the diabetic kidney in this study was not directly linked to severity, and thus, the altered response to oxygen supply may enable a further differentiation of the metabolic phenotype by interrogating the underlying mechanism, thus providing a window of opportunity for pharmacologically targeting these metabolically different phenotypes. In fact, recent studies have indicated that increased glycolytic flux as a renal protective trait and thus the phenotype seen here might be better protected against renal impairment (34). The alanine-to-total carbon ratio, regulated by the alanine transferase and linked via the cosubstrate glutamate and α-ketoglutarate to the glutamine and fatty acid synthesis, is insensitive to the changes in inhaled oxygen. This lack of oxygen dependency indicates a generally sufficient oxygen availability to maintain the increased mitochondrial fatty acid oxidation in kidney tubular cells (35) and similarly the bicarbonate-to-total carbon ratio that describes the oxidative phosphorylation via the mitochondrial pyruvate dehydrogenase activity (2-4). The oxygen-sensitive BOLD MRI showed hypoxia and increased oxygen consumption. These measurements indicate that a general deranged metabolism is inversely dependent on oxygen availability in the severe pseudohypoxic diabetic kidney, both with and without insulin treatment. Therefore, we suggest that the sensitivity toward changes in oxygen supply defines an alternative diabetic phenotype, indicating reduction in active cellular uptake of pyruvate. A potential limitation in the study design is the use of CSI for spatial localization of the metabolites, limiting the spatial resolution and especially the temporal resolution compared with faster or higher resolution imaging methods (26, 36-39). Another limitation is the need for anesthetics, which have been shown to impact the renal metabolism (40), although the used regime has only mild renal effects compared with other anesthetic regimes. Insulin administration did not alter the overall metabolic phenotype, which is supported by previous studies in heart and kidneys (20, 41, 42). However, it is important to note that the used insulin treatment was a dose mimicking suboptimal insulin treatment similar to a previous report (20), and as such, it is currently unknown what the impact of adequate insulin administration for sufficient glycemic control would entail. Further, 66% oxygen was chosen to ensure fully saturated blood, thus maximizing the potential differences between hypoxia and hyperoxia. No difference was observed between the results of this study in healthy controls and previous reports in controls and diabetics under normoxia and hyperoxia (100%) (3), and thus, it is unlikely that hyperoxia (66% O_2 in inspired air) was significantly contributing to the higher lactate production seen in the diabetic rats. Hyperglycemia-induced ketosis could be another potential confounding factor in the metabolic phenotypes, although rarely seen in the animal model used in this study (43); individual metabolic states could be a contributing factor in the increased variance seen in the diabetic rats.

In conclusion, the altered metabolic phenotype, manifested as significantly altered oxygen sensitivity in the presence of high intrarenal lactate levels, shows the existence of two seemingly different metabolic phenotypes in the diabetic kidney, which may highlight the need for tailored treatment strategies to reduce the impact of diabetes on long-term kidney function.

ACKNOWLEDGMENTS

The study was supported by The Simon Spies Foundation and the Danish National Research Foundation. Sascha Gude is acknowledged for her laboratory assistance.

Disclosures: No disclosures to report.

Conflict of Interest: The authors have no conflict of interest to declare.

REFERENCES

1. Brownlee M. Biochemistry and molecular cell biology of diabetic complications. Nature. 2001;414:813–820.
2. Palm F, Hansell P, Ronquist G, Waldenstr m A, Liss P, Carlsson PO. Polyol-pathway-dependent disturbances in renal medullary metabolism in experimental insulin-deficient diabetes mellitus in rats. Diabetologia. 2004;47:1223–1231.
3. Laustsen C, Lycke S, Palm F, Ostergaard JA, Bibby BM, Norregaard R, Flyvbjerg A, Pedersen M8, Ardenkjaer-Larsen JH. High altitude may alter oxygen availability and renal metabolism in diabetics as measured by hyperpolarized [1-13C]pyruvate magnetic resonance imaging. Kidney Int. 2014;86:67–74.
4. Laustsen C, Østergaard JA, Lauritzen MH, Nørregaard R, Bowen S, Søgaard LV, Flyvbjerg A, Pedersen M, Ardenkjaer-Larsen JH. Assessment of early diabetic renal changes with hyperpolarized [1-13C]pyruvate. Diabetes Metab Res Rev. 2013;29:125–129.
5. Laustsen C. Hyperpolarized renal magnetic resonance imaging: potential and oitfalls. Front Physiol. 2016;7:72.
6. Williamson JR, Chang K, Frangos M, Hasan KS, Ido Y, Kawamura T, Nyengaard JR, van den Enden M, Kilo C, Tilton RG. Hyperglycemic pseudohypoxia and diabetic complications. Diabetes. 1993;42:801–813.
7. Zhang G, Darshi M, Sharma K. The Warburg effect in diabetic kidney disease. Semin Nephrol. 2018;38:111–120.
8. Wolf M, de Boer A, Sharma K, Boor P, Leiner T, Sunder-Plassmann G, Moser E, Caroli A, Jerome NP. Magnetic resonance imaging T1- and T2-mapping to assess renal structure and function: a systematic review and statement paper. Nephrol Dial Transplant. 2018;33:ii41–ii50.
9. Caroli A, Schneider M, Friedli I, Ljimani A, De Seigneux S, Boor P, Gullapudi L8, Kazmi I, Mendichovszky IA, Notohamiprodjo M, Selby NM, Thoeny HC, Grenier N, Vallée JP. Diffusion-weighted magnetic resonance imaging to assess diffuse

renal pathology: a systematic review and statement paper. Nephrol Dial Transplant. 2018;33:ii29–ii40.
10. Pruijm M, Mendichovszky IA, Liss P, Van der Niepen P, Textor SC, Lerman LO, Krediet CTP, Caroli A, Burnier M, Prasad PV. Renal blood oxygenation level-dependent magnetic resonance imaging to measure renal tissue oxygenation: a statement paper and systematic review. Nephrol Dial Transplant. 2018;33:ii22–ii8.
11. Odudu A, Nery F, Harteveld AA, Evans RG, Pendse D, Buchanan CE, Francis ST, Fernández-Seara MA. Arterial spin labelling MRI to measure renal perfusion: a systematic review and statement paper. Nephrol Dial Transplant. 2018;33:ii15–ii21.
12. Boor P, Perkuhn M, Weibrecht M, Zok S, Martin I.V., Gieseke J, Schoth F, Ostendorf T, Kuhl C, Floege J. Diffusion-weighted MRI does not reflect kidney fibrosis in a rat model of fibrosis. J Magn Reson Imaging. 2015;42:990–998.
13. Friedli I, Crowe LA, Berchtold L, Moll S, Hadaya K, de Perrot T, Vesin C, Martin PY, de Seigneux S, Vallée JP. New magnetic resonance imaging index for renal fibrosis assessment: A comparison between diffusion-weighted imaging and T1 mapping with histological validation. Sci Rep. 2016;6:30088.
14. Laustsen C, Stokholm Norlinger T, Christoffer Hansen D, Qi H, Mose Nielsen P, Bonde Bertelsen L, Henrik Ardenkjaer-Larsen J, Stødkilde Jørgensen H. Hyperpolarized 13C urea relaxation mechanism reveals renal changes in diabetic nephropathy. Magn Reson Med. 2016;75:515–518.
15. Pedersen M, Dissing TH, Morkenborg J, Stodkilde-Jorgensen H, Hansen LH, Pedersen LB, Grenier N, Frøkiaer J. Validation of quantitative BOLD MRI measurements in kidney: application to unilateral ureteral obstruction. Kidney Int. 2005; 67:2305–2312.
16. Ardenkjaer-Larsen JH, Fridlund B, Gram A, Hansson G, Hansson L, Lerche MH, Servin R, Thaning M, Golman K. Increase in signal-to-noise ratio of >10,000 times in liquid-state NMR. Proc Natl Acad Sci U S. 2003;100:10158–10163.
17. Nelson SJ, Kurhanewicz J, Vigneron DB, Larson PEZ, Harzstark AL, Ferrone M, van Criekinge M, Chang JW, Bok R, Park I, Reed G, Carvajal L, Small EJ, Munster P, Weinberg VK, Ardenkjaer-Larsen JH, Chen AP, Hurd RE, Odegardstuen LI, Robb FJ, Tropp J, Murray JA. Metabolic imaging of patients with prostate cancer using hyperpolarized [1-^{13}C]pyruvate. Sci Transl Med. 2013;5:198ra08.
18. Kurhanewicz J, Vigneron DB, Brindle K, Chekmenev EY, Comment A, Cunningham CH, Deberardinis RJ, Green GG, Leach MO, Rajan SS, Rizi RR, Ross BD, Warren WS, Malloy CR. Analysis of cancer metabolism by imaging hyperpolarized nuclei: prospects for translation to clinical research. Neoplasia. 2011;13: 81–97.
19. Kurhanewicz J, Vigneron DB, Ardenkjaer-Larsen JH, Bankson JA, Brindle K, Cunningham CH, Gallagher FA, Keshari KR, Kjaer A, Laustsen C, Mankoff DA, Merritt ME, Nelson SJ, Pauly JM, Lee P, Ronen S, Tyler DJ, Rajan SS, Spielman DM, Wald L, Zhang X, Malloy CR, Rizi R. Hyperpolarized (13)C MRI: path to clinical translation in oncology. Neoplasia. 2018;21:1–16.
20. Laustsen C, Lipso K, Ostergaard JA, Norregaard R, Flyvbjerg A, Pedersen M, Palm F, Ardenkjær-Larsen JH. Insufficient insulin administration to diabetic rats increases substrate utilization and maintains lactate production in the kidney. Physiol Rep. 2014;2. pii: e12233.
21. Qi H, Nielsen PM, Schroeder M, Bertelsen LB, Palm F, Laustsen C. Acute renal metabolic effect of metformin assessed with hyperpolarised MRI in rats. Diabetologia. 2018;61:445–454.
22. Norlinger TS, Nielsen PM, Qi H, Mikkelsen E, Hansen K, Schmidt NH, Pedersen M, Agger P, Palm F, Laustsen C. Hyperbaric oxygen therapy reduces renal lactate production. Physiol Rep. 2017;5. pii: e13217.
23. von Morze C, Chang GY, Larson PE, Shang H, Allu PK, Bok RA, Crane JC, Olson MP, Tan CT, Marco-Rius I, Nelson SJ, Kurhanewicz J, Pearce D, Vigneron DB. Detection of localized changes in the metabolism of hyperpolarized gluconeogenic precursors 13 C-lactate and 13 C-pyruvate in kidney and liver. Magn Reson Med. 2017;77:1429–1437.
24. Morze CV, Allu PKR, Chang GY, Marco-Rius I, Milshteyn E, Wang ZJ, Ohliger MA, Gleason CE, Kurhanewicz J, Vigneron DB, Pearce D. Non-invasive detection of divergent metabolic signals in insulin deficiency vs. insulin resistance in vivo. Sci Rep. 2018;8:2088.
25. Laustsen C, Nielsen PM, Norlinger TS, Qi H, Pedersen UK, Bertelsen LB, Østergaard JA, Flyvbjerg A, Ardenkjær-Larsen JH, Palm F, Stødkilde-Jørgensen H. Antioxidant treatment attenuates lactate production in diabetic nephropathy. Am J Physiol Renal Physiol. 2017;312:F192–F199.
26. Schmidt R, Laustsen C, Dumez JN, Kettunen MI, Serrao EM, Marco-Rius I, Brindle KM, Ardenkjaer-Larsen JH, Frydman L. In vivo single-shot 13C spectroscopic imaging of hyperpolarized metabolites by spatiotemporal encoding. J Magn Reson. 2014;240:8–15.
27. Halestrap AP, Wilson MC. The monocarboxylate transporter family–role and regulation. IUBMB Life. 2012;64:109–119.
28. Bellomo R. Bench-to-bedside review: lactate and the kidney. Crit Care. 2002;6: 322–326.
29. Khacho M, Tarabay M, Patten D, Khacho P, MacLaurin JG, Guadagno J, Bergeron R, Cregan SP, Harper ME, Park DS, Slack RS. Acidosis overrides oxygen deprivation to maintain mitochondrial function and cell survival. Nat Commun. 2014;5:3550.
30. McCommis KS, Finck BN. Mitochondrial pyruvate transport: a historical perspective and future research directions. Biochem J. 2015;466:443–454.
31. Philp A, Macdonald AL, Watt PW. Lactate – a signal coordinating cell and systemic function. J Exp Biol. 2005;208:4561–4575.
32. Xie J, Wu H, Dai C, Pan Q, Ding Z, Hu D, Ji B, Luo Y, Hu X. Beyond Warburg effect – dual metabolic nature of cancer cells. Sci Rep. 2014;4:4927.
33. Lin MH, Chen HY, Liao TH, Huang TC, Chen CM, Lee JA. Determination of time-dependent accumulation of D-lactate in the streptozotocin-induced diabetic rat kidney by column-switching HPLC with fluorescence detection. J Chromatogr B Analyt Technol Biomed Life Sci. 2011;879:3214–3219.
34. Qi W, Keenan HA, Li Q, Ishikado A, Kannt A, Sadowski T, Yorek MA, Wu IH, Lockhart S, Coppey LJ, Pfenninger A, Liew CW, Qiang G, Burkart AM, Hastings S, Pober D, Cahill C, Niewczas MA, Israelsen WJ, Tinsley L, Stillman IE, Amenta PS, Feener EP, Vander Heiden MG, Stanton RC, King GL. Pyruvate kinase M2 activation may protect against the progression of diabetic glomerular pathology and mitochondrial dysfunction. Nat Med. 2017;23:753–762.
35. Rosca MG, Vazquez EJ, Chen Q, Kerner J, Kern TS, Hoppel CL. Oxidation of fatty acids is the source of increased mitochondrial reactive oxygen species production in kidney cortical tubules in early diabetes. Diabetes. 2012;61:2074–2083.
36. Vinding MS, Laustsen C, Maximov I.I., Sogaard LV, Ardenkjaer-Larsen JH, Nielsen NC. Dynamic nuclear polarization and optimal control spatial-selective 13C MRI and MRS. J Magn Reson. 2013;227:57–61.
37. Gordon JW, Niles DJ, Fain SB, Johnson KM. Joint spatial-spectral reconstruction and k-t spirals for accelerated 2D spatial/1D spectral imaging of 13C dynamics. Magn Reson Med. 2014;71:1435–1445.
38. Milshteyn E, von Morze C, Gordon JW, Zhu Z, Larson PEZ, Vigneron DB. High spatiotemporal resolution bSSFP imaging of hyperpolarized [1-(13) C]pyruvate and [1-(13) C]lactate with spectral suppression of alanine and pyruvate-hydrate. Magn Reson Med. 2018;80:1048–1060.
39. Lau JYC, Geraghty BJ, Chen AP, Cunningham CH. Improved tolerance to off-resonance in spectral-spatial EPI of hyperpolarized [1-(13) C]pyruvate and metabolites. Magn Reson Med. 2018;80:925–934.
40. Qi H, Mariager CO, Lindhardt J, Nielsen PM, Stodkilde-Jorgensen H, Laustsen C. Effects of anesthesia on renal function and metabolism in rats assessed by hyperpolarized MRI. Magn Reson Med. 2018;80:2073–2080.
41. Lauritzen MH, Laustsen C, Butt SA, Magnusson P, Sogaard LV, Ardenkjaer-Larsen JH, Åkeson P. Enhancing the [13C]bicarbonate signal in cardiac hyperpolarized [1-13C]pyruvate MRS studies by infusion of glucose, insulin and potassium. NMR Biomed. 2013;26:1496–1500.
42. Hansen ESS, Tougaard RS, Norlinger TS, Mikkelsen E, Nielsen PM, Bertelsen LB, Bøtker HE, Jørgensen HS, Laustsen C. Imaging porcine cardiac substrate selection modulations by glucose, insulin and potassium intervention: a hyperpolarized [1-(13) C]pyruvate study. NMR Biomed. 2017;30.
43. Forster O, Rudas B. Ketosis in rats with streptozotocin-induced diabetes. Lancet. 1969;1:1321–1322.